J Solid State Electrochem (2011) 15:2331–2339
DOI 10.1007/s10008-011-1446-0

ORIGINAL PAPER

Influence of ultrathin poly-(3,4-ethylenedioxythiophene) (PEDOT) film supports on the electrodeposition and electrocatalytic activity of discrete platinum nanoparticles

Hollie V. Patten · Edgar Ventosa · Alvaro Colina · Virginia Ruiz · Jesús López-Palacios · Andrew J. Wain · Stanley C. S. Lai · Julie V. Macpherson · Patrick R. Unwin

Received: 25 March 2011 / Revised: 10 May 2011 / Accepted: 10 May 2011 / Published online: 11 June 2011

Abstract Coating a carbon electrode surface, specifically highly oriented pyrolytic graphite (HOPG) with an ultrathin film of poly-(3,4-ethylenedioxythiophene), PEDOT, provides a support on which a high density of uniformly dispersed Pt nanoparticles (NPs) can readily be formed by electrodeposition. The NPs tend to be much smaller, have a higher surface coverage, better dispersion and show a much lower tendency to aggregate, than Pt NPs produced under identical electrochemical conditions on HOPG alone. The electrocatalytic activity of the NPs was investigated for methanol (MeOH) and formic acid (HCOOH) oxidation. Significantly, for similarly prepared particles, Pt NP-PEDOT arrays exhibited higher catalytic activity (in terms of current density, based on the Pt area), towards MeOH oxidation, by an order of magnitude, and towards HCOOH oxidation at high potentials, than Pt NPs supported on native HOPG. These findings can be rationalised in terms of the enhanced oxidation of adsorbed CO, a key reaction intermediate and a catalyst poison. This research provides strong evidence that employing conducting polymers, such as PEDOT, as a support substrate, can greatly improve particular catalytic reactions, allowing for better catalyst utilisation in fuel cell technology.

Keywords Electrocatalysis · Methanol oxidation · Formic acid oxidation · HOPG · PEDOT · Pt NPs

Dedicated to Professor George Inzelt on the occasion of his 65th birthday.

H. V. Patten · E. Ventosa · S. C. S. Lai · J. V. Macpherson · P. R. Unwin (✉)
Department of Chemistry, University of Warwick,
Coventry CV4 7AL, UK
e-mail: p.r.unwin@warwick.ac.uk

E. Ventosa · A. Colina · J. López-Palacios
Departamento de Química, Universidad de Burgos,
Pza. Misael Bañuelos s/n,
09001 Burgos, Spain

V. Ruiz
Centro de Tecnologías Electroquímicas,
Parque Tecnológico de San Sebastián,
Paseo Miramón 196,
20009 San Sebastián, Spain

A. J. Wain
National Physical Laboratory,
Teddington,
Middlesex TW11 0LW, UK

Introduction

Key components of fuel cells are the electrocatalyst and support material. Metal nanoparticles (NPs), typically Pt or Pt–alloys [1, 2], are often employed as the catalyst, usually immobilised on a carbon support. Elucidating the size dependence of electrocatalysis at NPs is of considerable interest [3, 4]. Small NPs provide a large area-to-volume ratio which is beneficial for achieving efficient catalyst use, provided there is no reduction in the efficacy of the surface catalytic process. An important consideration is that decreasing the catalyst size may also induce changes in the electronic properties of the particles, which, in turn, may influence their catalytic activity [5]. In addition to particle size effects, the structure and morphology of supported electrocatalysts are also important factors [6–8].

The development of catalyst dispersion methods and supports for catalytic NPs is of significant interest [9]. It is well-known that the material employed as catalyst support plays an essential role in catalyst activity and stability [10, 11]. While carbon materials are most widely used as support materials, conducting polymers (CPs) have also shown great promise [12–17]. Nanocomposites of CPs and NPs have been shown to improve the adherence of NPs to solid electrodes and may impart synergetic electrocatalytic properties [18, 19], notably when employed in the direct methanol fuel cell [15] and the direct formic acid fuel cell [20].

Methanol (MeOH) oxidation involves several possible pathways, each comprising a number of elementary steps (Fig. 1), as described by Baltruschat et al. [21, 22] and Léger [23]. The oxidation of MeOH can proceed via adsorbed CO (CO_{ads}) (step 1). Although CO_{ads} can be further oxidised to CO_2 (step 2), this reaction is sluggish and requires a high overpotential [24–26]. As a result, CO_{ads} is generally considered a poison in the methanol oxidation mechanism. Alternatively, the reaction may proceed via soluble intermediates such as formic acid (HCOOH; steps 3 and 4). HCOOH oxidation can also occur through more than one pathway resulting in direct oxidation to CO_2 (step 5) or through CO_{ads} (steps 2 and 6) [27–29]. This multitude of possible reaction pathways highlights the importance of optimising fuel cell catalyst layers through the assessment of Pt NP electrocatalytic activity in different environments. A previous study showed that by modifying electrodeposited Pt on glassy carbon electrode with polyindoles, the electrocatalytic activity towards formic acid oxidation was increased. This was attributed to the polyindoles providing a selective pathway, suppressing the formation of CO. This indicated a possible synergetic effect between Pt and polyindoles [30].

Among CPs, poly-(3,4-ethylenedioxythiophene) (PEDOT) has considerable promise as a support for Pt NPs, with enhanced catalytic activity of Pt–PEDOT composites compared to native Pt suggested for the electrooxidation of MeOH [31, 32]. However, the preparation techniques employed in these previous studies resulted in extensive aggregation of NPs, making it difficult to determine the intrinsic activity at the single, isolated particle level and, in particular, elucidate whether PEDOT plays any role in promoting electrocatalysis. In a contrasting report, Pt NP composites with either polypyrrole or PEDOT demonstrated comparable activities towards MeOH oxidation as for a bare Pt electrode [33]. Finally, there is recent evidence for the promotion of electrocatalytic activity for ethanol oxidation by embedding Pd NPs in a PEDOT matrix [34]. In view of the current status of the field, studies with well-defined, non-aggregated Pt NPs are required to elucidate whether PEDOT enhances electrocatalysis at Pt NPs. Such studies are a major focus of this paper which seeks to compare directly the electrocatalytic activity of isolated, well-defined, Pt NPs on: (1) highly oriented pyrolytic graphite (HOPG) and (2) on molecularly smooth ultrathin films of PEDOT. Through these studies, we are able to determine the influence of PEDOT on enhancing, or otherwise modifying, the activity of Pt NPs towards MeOH and HCOOH oxidation.

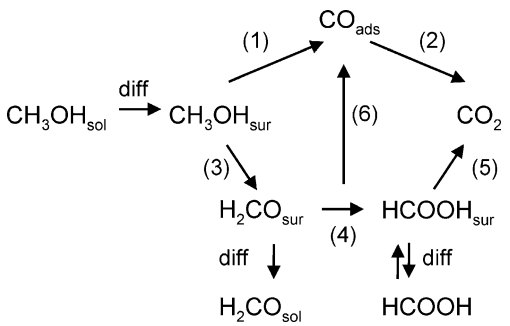

Fig. 1 Schematic showing the different pathways for MeOH oxidation. Adapted from Baltruschat et al. [21]

Electrodeposition is an attractive route for the formation of tailored nanostructured interfaces, as it provides versatility in the range of particle sizes and surface coverages that can be obtained [35–37]. On the other hand, because such particles are unprotected, there is a tendency for aggregation to occur, and on solid surfaces nucleation and growth may take place at specific locations (e.g. at step edges) leading to non-uniform surface coverages [38, 39]. In this work, we show that a further beneficial aspect of PEDOT, as a support, is that it is possible to readily form high-density arrays of small isolated NPs using electrodeposition at molecularly smooth CP films [40]. The NPs tend to be much smaller and can be deposited with much better dispersion than on bare HOPG.

In this work, the use of such Pt NP-PEDOT arrays for electrocatalysis has been considered through studies of the electrooxidation of MeOH and HCOOH. We are most interested in comparing the activities (in terms of current density) of the different nanostructured interfaces. To this end, the activity of Pt NP-PEDOT has been compared with similarly prepared Pt NPs on HOPG, to fully elucidate the effect of a PEDOT support on heterogeneous electrocatalytic reactions.

Experimental

Materials

All aqueous solutions were prepared from Milli-Q reagent water (Millipore Corp.) with resistivity of 18.2 MΩ cm at 25 °C. The supporting electrolytes were: 0.1 M $LiClO_4$ (Aldrich ACS) for electropolymerization, 0.25 M $HClO_4$

(Acros Organics) for NP electrodeposition and 0.2 M H_2SO_4 (Fisher Scientific Reagent Grade) for studies of the electrooxidation of MeOH and HCOOH. The monomer 3,4-ethylenedioxythiophene (EDOT, Aldrich), potassium hexachloroplatinate (K_2PtCl_6, Aldrich), methanol (Fisher Scientific Reagent Grade), and formic acid (Aldrich Reagent Grade) were all used as received.

Atomic force microscopy

Tapping mode (TM)-atomic force microscopy (AFM) measurements were performed in air using standard Si tapping tips (RSEFP-type Veeco Probes) with a Multimode VAFM (Veeco). Images were analysed using SPIP software, version 5.1.5 (Image Metrology).

Electrochemistry

Cyclic voltammetry (CV), linear sweep voltammetry (LSV), and chronoamperometry experiments employed a potentiostat (CH Instruments, model CHI760A) in a three-electrode configuration, with SPI-1 grade HOPG (Structure Probe Inc.) as the working electrode, a Pt sheet counter electrode and a Ag/AgCl (3 M KCl) reference electrode (World Precision Instruments 2SH-DRIREF), against which all potentials are quoted. A 10×10 mm sample of HOPG was placed onto a square section of Au-sputtered silicon (sputter-coated (Moorfield minibox conversion) thickness 400 nm), with an underlying electrical contact made using silver DAG (Ag-loaded epoxy, Agar Scientific). Finally, tinned copper wire was soldered to the coated silicon chip in order to make external electrical contact. Prior to any electrochemistry, the HOPG was cleaved revealing a fresh surface, using Scotch tape (3M). For studies on PEDOT, molecularly smooth films were produced on HOPG as outlined previously [40], by applying a potential step from +0.5 to +1.05 V for 0.1 s in a 0.002 M EDOT and 0.1 M $LiClO_4$ solution. As demonstrated elsewhere [40], growth is governed by a 2-D layer-by-layer process at these low driving forces. The films produced under these conditions typically had a thickness of *ca.* 8 nm [40].

Results and discussion

Electrodeposition of Pt NPs on bare and PEDOT-coated HOPG

The electrochemical nucleation and growth of metal NPs on conducting substrates can be controlled by three parameters; the concentration of the metal salt, deposition potential, and deposition time [41]. The last two parameters can be combined by the use of complex potential waveforms [35]. In this study, we mainly considered simple single potential step chronoamperometry, with a deposition time of 10 s in order to elucidate clearly the effect of PEDOT on NP formation. The effect of the salt concentration and deposition potential were investigated. For Pt electrodeposition, the electrode potential was stepped from +0.5 V to a series of different driving potentials in the range −0.1 to −0.4 V. The solution comprised 0.25 M $HClO_4$ with different concentrations of K_2PtCl_6 in the range 1–9 mM. For all driving potentials and timescales, a concentration of 3 mM K_2PtCl_6 was found to give rise to the highest NP surface coverage on PEDOT films without obvious aggregation; however, aggregation was seen at higher concentrations. We thus focused further on these conditions.

TM-AFM was employed to obtain information on particle size (from maximum height), the particle surface coverage and to determine if there were any preferential sites for deposition on the surfaces of interest. To directly compare Pt electrodeposition on bare and PEDOT-coated HOPG, particles were deposited using chronoamperometry by stepping the potential from 0.5 V to cathodic potentials (10 s). Typical data for a deposition potential of −0.2 V are shown in Fig. 2. On the PEDOT-coated HOPG (Fig. 2a), the average particle size is 14±5 nm and the surface coverage is *ca.* nine particles per square micrometer. The image revealed an essentially homogenous dispersion of NPs and no preferential deposition sites on the support electrode. In contrast, for identical deposition parameters, Pt particles electrodeposited on bare HOPG (Fig. 2b) had an average particle size of 94± 17 nm and a coverage of two particles per square micrometer. In general, much larger NP sizes (mainly aggregates) and considerably smaller surface coverages were found on HOPG, with some preferential deposition at step edges. This indicates that the PEDOT film readily promotes the nucleation of a high density of small NPs compared to a bare HOPG electrode. For Pt NPs deposited on PEDOT-coated HOPG, the particle size decreased when the deposition potential was changed from −0.2 to −0.1 V, but small particles could be produced most readily at potentials beyond −0.3 V, due to the concomitant H_2 evolution reaction (HER) which essentially inhibits the electrodeposition process (see Table 1).

Validation of NP geometry and the use of AFM for the estimation of NP surface coverages

Deposition of NPs and metal oxide nanowires on HOPG has been shown to occur preferentially at step edges [42] or where a reaction can be driven to decorate steps [36, 43]. Since each cleaved surface of HOPG has a different step density, AFM characterisation of every surface was neces-

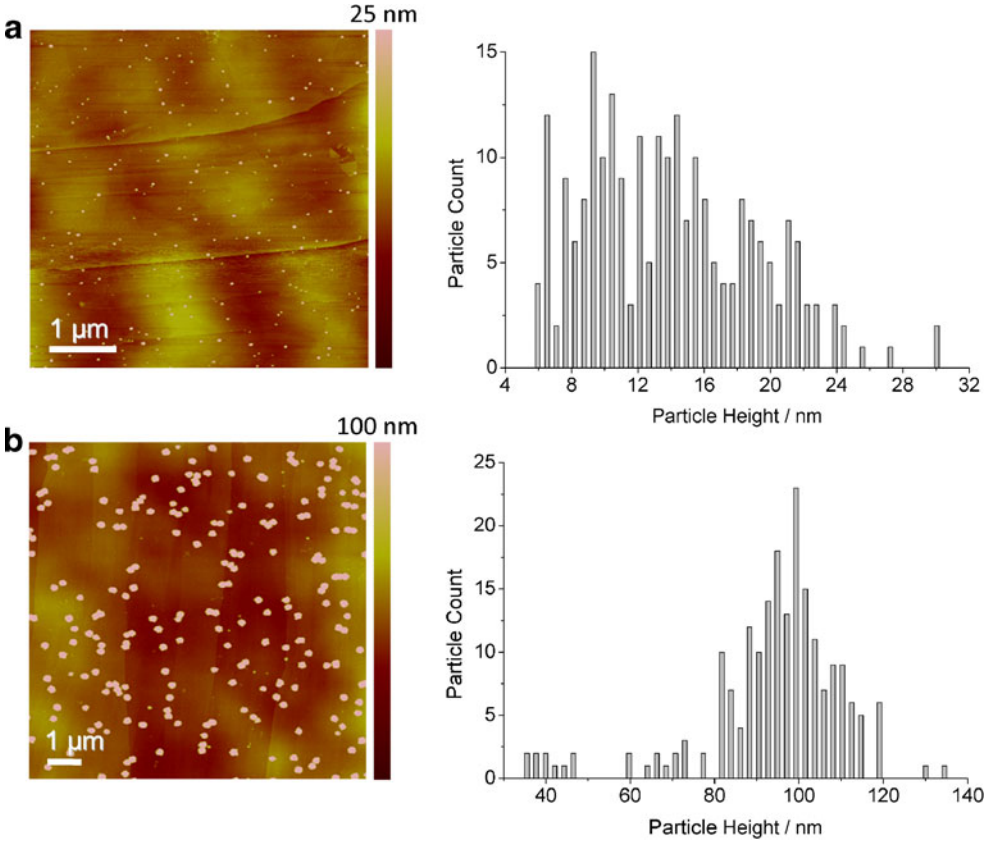

Fig. 2 Tapping mode AFM images of Pt NPs deposited from a solution of 3 mM K_2PtCl_6 (0.25 M $HClO_4$) with a potential step from 0.5 to −0.2 V (10 s) on: **a** PEDOT coated-HOPG and **b** bare HOPG. Note the difference in the height scales for the two images

sary after forming the Pt NP arrays and performing electrochemistry. This ensured that the electrocatalysis characteristic of each freshly prepared surface could be correlated directly with catalyst loading.

Previous studies have demonstrated good agreement between particle sizes determined from the deposition charge and those measured by AFM [44]. Other studies have calculated the Pt coverage of a surface using the charge of the Pt oxide stripping peak [45] and the charge of the hydrogen underpotential deposition (hydrogen adsorption; H_{ads}) peaks [46]. Determination of the Pt area using these classical methods was not always possible for the studies herein because of the small geometric area together with the low loading. Furthermore, the use of the charge passed during electrodeposition to estimate the amount of Pt electrodeposited was compromised by the HER when producing the smallest NPs [31]. However, under certain deposition conditions, where the charge from the Pt oxide stripping peak and/or H_{ads} peaks was measurable, the AFM approach to determine Pt surface coverage could be validated. For example, for NPs electrodeposited on HOPG from 3 mM K_2PtCl_6 (0.25 M $HClO_4$) at −0.3 V (10 s) so that a reasonably high surface coverage was produced (Fig. 3a), it was possible to show that the surface coverages estimated by AFM and CV (Fig. 3b) were in good agreement.

Table 1 Pt NP height and number of NPs for electrodeposition on native HOPG and PEDOT coated-HOPG

	Native HOPG		PEDOT	
Potential (V) applied (10 s) for deposition of Pt	NP height (nm)	Number of NPs (μm^{-2})	NP height (nm)	Number of NPs (μm^{-2})
−0.1			15±9	5
−0.2	94±17	2	14±5	9
−0.3	41±30	5	4±3	69
−0.4			6±4	86

CV was performed immediately after deposition of NPs using a fresh aqueous solution containing 0.2 M H_2SO_4 with a scan rate of 0.5 V/s (Fig. 3b). For this particular case, the surface coverages (active Pt area/electrode geometric area) determined were: (1) Pt oxide stripping 4.8±0.2%, (2) H_{ads} 5±0.5%, and (3) AFM 4.2±0.4%. The AFM value is based on a spherical, rather than hemispherical, NP geometry for which the NP height is equivalent to the NP diameter rather than the NP radius; assumption of a hemispherical NP gave poor agreement. This was confirmed in two further experiments; thus, comparison of the AFM and CV data indicate NPs have a geometry that is close to spherical.

It was not possible to make surface area measurements based on voltammetric methods (Pt oxide stripping or

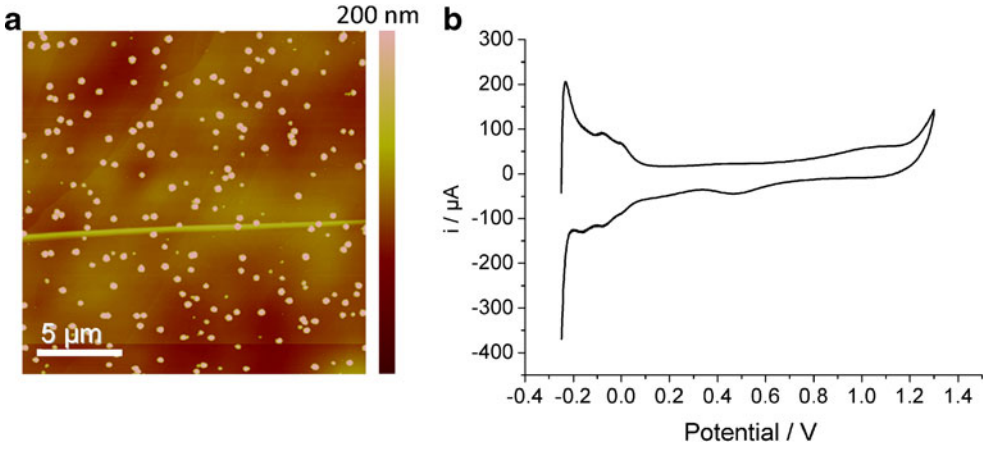

Fig. 3 Tapping mode AFM image of Pt NPs deposited from a solution of 3 mMK_2PtCl_6 (0.25 M $HClO_4$) following a potential step from 0.5 to −0.3 V (10 s) on bare HOPG (**a**) height image (**b**); CV to show both the Pt oxide stripping peak and H_{ads} peaks for the Pt-HOPG array electrode using 0.2 M H_2SO_4 with a scan rate of 0.5 Vs^{-1}

hydrogen adsorption) on PEDOT-coated HOPG because of more sizeable background processes from the conducting polymer film. However, it is important to point out that the assumption of a hemispherical, rather than spherical geometry for the Pt NPs, would mean using the AFM height data as the hemisphere radius and this would increase the surface area by a factor of 2 compared to the spherical case (with the height as the particle diameter). As shown herein, even this maximum level of uncertainty in the NP geometry cannot account for the dramatic difference in the activity of Pt NPs on HOPG and PEDOT-HOPG reported in section "Electrooxidation of methanol".

Electrocatalytic activity of Pt-PEDOT and Pt-HOPG

Both MeOH and HCOOH oxidation were investigated to assess whether an intervening PEDOT film between HOPG and the Pt NPs had any effect on the resulting electrocatalytic activity, compared to bare HOPG, for similarly prepared NPs. The peak currents for these electrochemical processes during LSV at 50 mV s^{-1} were typically background corrected (by performing CV on the substrate with aqueous 0.2 M H_2SO_4 and subtracting this from the response with MeOH or HCOOH present) and normalised by the mean surface area of deposited platinum (determined by AFM image analysis as outlined in section "Validation of NP geometry and the use of AFM for the estimation of NP surface coverages"). Because of the Pt aggregation issue on HOPG and the fact that each freshly cleaved surface can vary in terms of step density, the protocol for Pt electrodeposition was established by trial and error to create a Pt NP size on HOPG as close as possible to that on PEDOT.

Electrooxidation of methanol

The activity of Pt-HOPG (Fig. 4) and Pt-PEDOT (Fig. 5) arrays for the electrooxidation of MeOH was investigated by performing LSV measurements between 0.0 and +0.90 V in a solution containing 0.1 M MeOH and 0.2 M H_2SO_4. The LSV shape for MeOH oxidation, with a peak located at *ca*. +0.6 V (shown in Figs. 4c and 5c) was similar for both surfaces. The average MeOH oxidation peak current for Pt-HOPG was found to be 470±160 μA cm^{-2} (n=3; 1 SD). This value is comparable to previous studies of MeOH oxidation employing HOPG or GC as a support for Pt NPs [47–49].

Interestingly, a much increased activity, by a factor of ten, was observed for the Pt-PEDOT surfaces with an average activity of 5.1±1.2 mA cm^{-2} Pt (n=3; 1 SD). Figure 4 gives an example of results using a Pt NP-HOPG substrate with an average NP diameter of 36±13.5 nm (6.5 particles per square micrometer) and an activity of 230 μA cm^{-2} Pt (Fig. 4c), whilst Fig. 5 demonstrates the same reaction for a Pt NP-PEDOT surface with average NP diameter of 15.5±7.7 nm (9.8 particles per square micrometer) and an activity of 6.3 mA cm^{-2} Pt. It is important to note that although the NPs differ in size by a factor of two, NP size effect are not anticipated for NPs of this size range [50, 51]. Furthermore, size effects could not account for the order of magnitude difference in the current density that is evident.

Electrooxidation of formic acid

In addition to methanol oxidation, the effect of PEDOT was also studied for HCOOH oxidation. Both in the absence and in the presence of a PEDOT film, a current peak was observed at *ca.* +0.3 V. Furthermore, an additional shoulder was observed at *ca.* +0.65 V, in the presence of PEDOT.

Typical AFM images of Pt electrodeposited on both Pt-HOPG and Pt-PEDOT, along with the corresponding LSV response for HCOOH oxidation are shown in Figs. 6 and 7, respectively. Figure 6 shows a HOPG surface with an average Pt particle diameter of 13.0±3.8 nm (four particles per square micrometer) with an activity of 7.9 mA cm^{-2} Pt at the peak at 0.3 V, whereas Fig. 7 shows a Pt NP-PEDOT

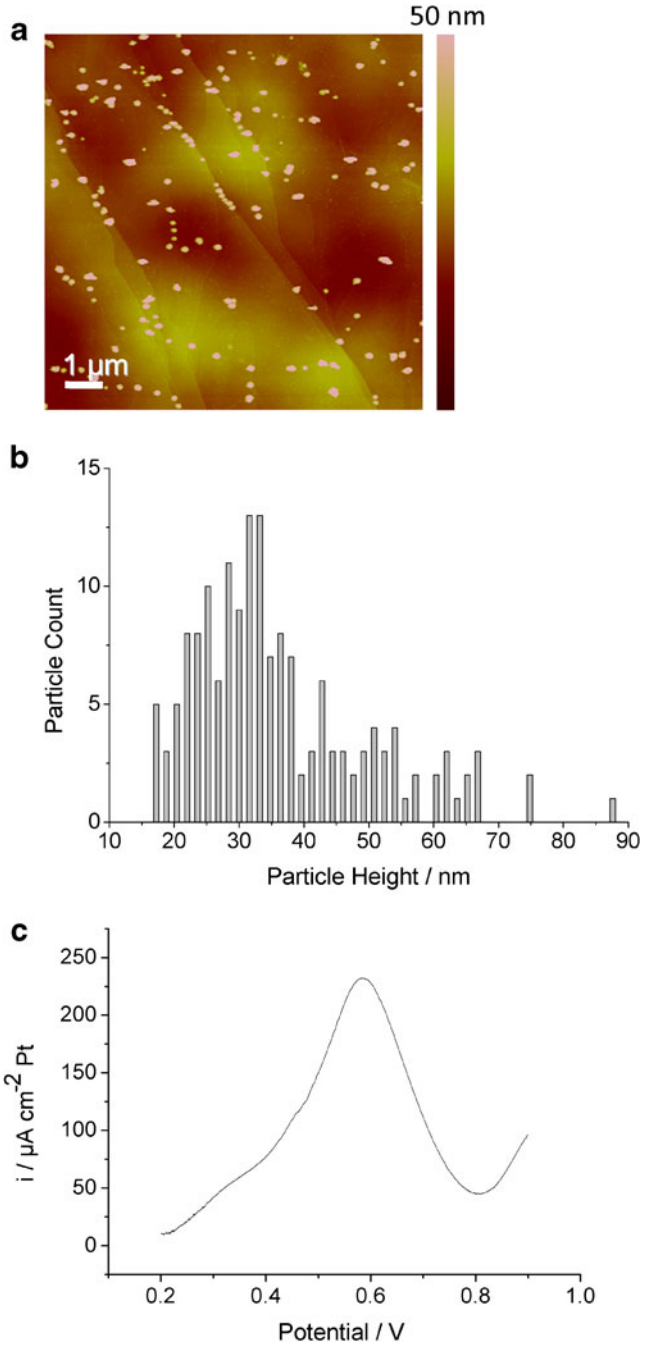

Fig. 4 Example analysis for MeOH oxidation at Pt NP-HOPG. **a** Tapping mode AFM image, **b** particle size distribution, and **c** LSV (0.05 $V s^{-1}$) for methanol oxidation in 0.1 M MeOH and 0.2 M H_2SO_4

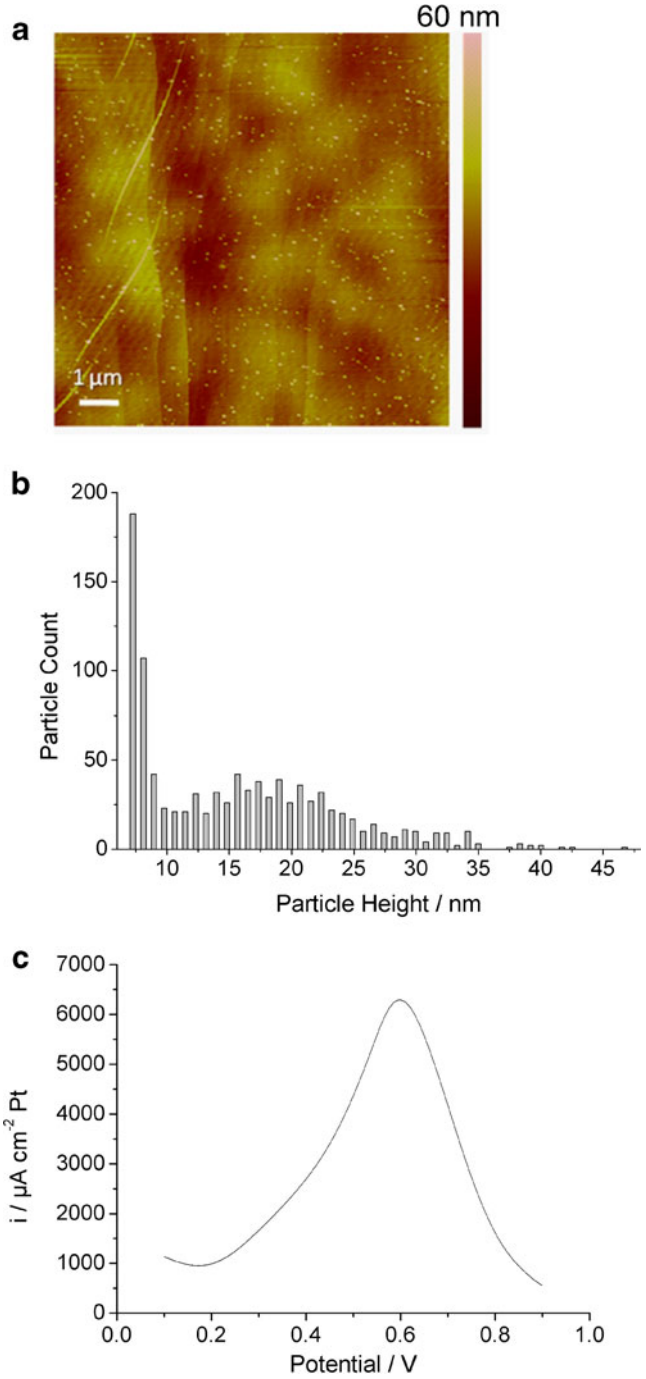

Fig. 5 Example analysis for MeOH oxidation at Pt NP-PEDOT array. **a** Tapping mode AFM image, **b** particle size distribution, and **c** LSV (0.05 $V s^{-1}$) for methanol oxidation in 0.1 M MeOH and 0.2 M H_2SO_4

surface where the average particle diameter is 13.9±5.1 nm (nine particles per square micrometer) with an activity of 5.8 mA cm^{-2} Pt at the peak at 0.3 V. From three separate experiments on each type of surface, the activities (and particle sizes) for Pt-HOPG and Pt-PEDOT were 6.5± 1.4 mA cm^{-2} Pt (n=3; 1 SD; 16.8±6.8 nm) and 5.9± 0.6 mA cm^{-2} Pt (n=3; 1 SD; 14.4±6.4 nm), respectively. Thus, in terms of the first peak the current density on Pt-PEDOT and Pt NPs was similar. However, a significant activity at higher potentials (above 0.5 V) was also observed in the presence of PEDOT which was negligible on native HOPG. Thus, the PEDOT support greatly influences the electrocatalytic activity and the reasons for this are considered below.

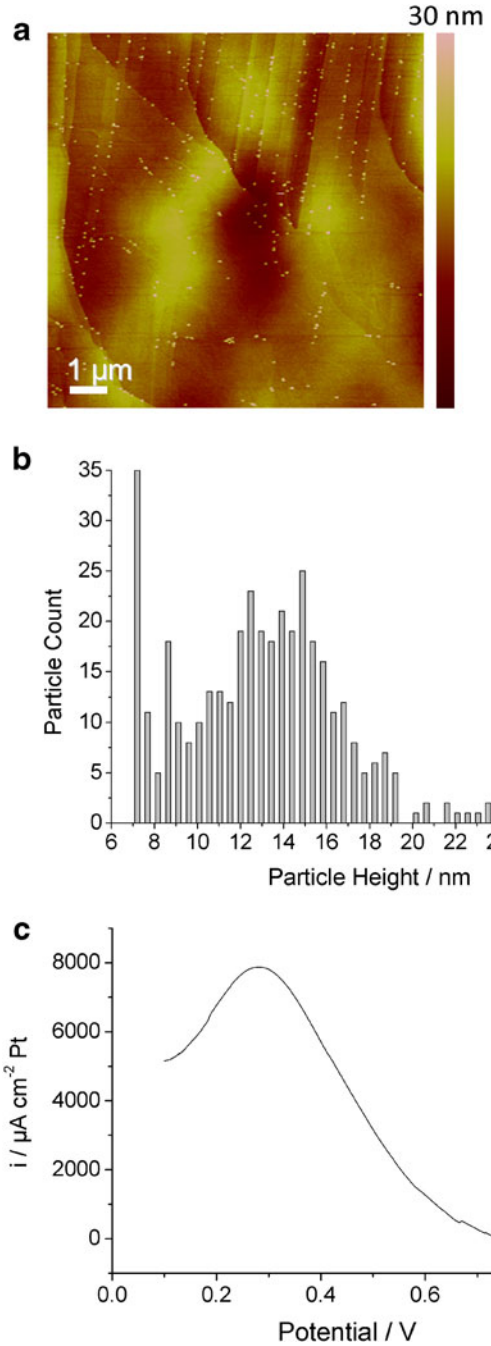

Fig. 6 Example analysis for formic acid oxidation at Pt NP-HOPG. **a** Tapping mode AFM image, **b** particle size distribution, **c** LSV (0.05 V s^{-1}) for formic acid oxidation in 0.1 M HCOOH and 0.2 M H_2SO_4

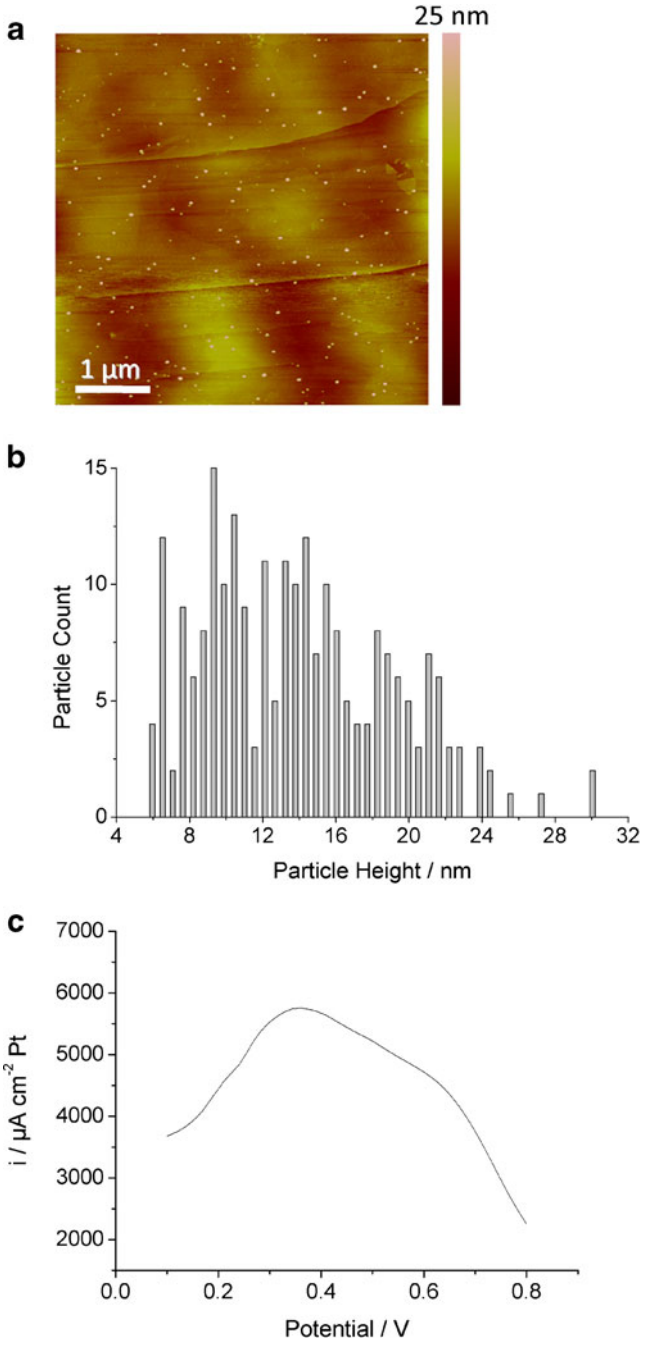

Fig. 7 Example analysis for formic acid oxidation at Pt NP-PEDOT. **a** Tapping mode AFM image, **b** particle size distribution, **c** LSV (0.05 V s^{-1}) for formic acid oxidation in 0.1 M HCOOH and 0.2 M H_2SO_4

General discussion

Based on the results described in the previous section, it is clear that the presence of a PEDOT film alters the electrocatalytic activity of HOPG supported platinum nanoparticles towards MeOH and HCOOH oxidation significantly. In the case of MeOH oxidation, the PEDOT film increases the currents by an order of magnitude while keeping the shape of the voltammetric profile unaltered. On the other hand, for HCOOH oxidation, both the magnitude (currents) and the shape of the voltammetric profile are altered by the presence of a PEDOT film. To understand this markedly different effect of the PEDOT film, it is necessary to consider the complex oxidation mechanism of MeOH and HCOOH (Fig. 1), as discussed in the "Introduction" section.

In the absence of PEDOT, it is well-known that methanol and formic acid decompose at low potentials to form

strongly adsorbed CO (reactions 1 and 6) [52]. As the oxidative removal of CO_{ads} on platinum in sulfuric acid does not occur at potentials below 0.4–0.5 V (vs. Ag/AgCl) [24, 26], this indicates that at low potentials the platinum electrocatalyst will be partially covered by a CO adlayer. In the absence of PEDOT, MeOH oxidation is mostly inhibited by this CO adlayer (as witnessed by the low currents observed below 0.4 V) and significant currents are only obtained at higher potentials at which oxidation of the poisoning CO_{ads} occurs, as can be seen in the voltammogram in Fig. 4c. HCOOH oxidation, however, can take place at a partially blocked surface (Fig. 6c), indicating that HCOOH oxidation (through reaction 5 in Fig. 1, as reaction 2 does not occur at low potentials) is less "site-demanding" than MeOH oxidation.

The presence of PEDOT does not significantly alter the voltammetric responses below 0.4 V: MeOH oxidation is still blocked (Fig. 5c), while HCOOH oxidation (through reaction 5) still occurs at the same effective rate, indicating that the PEDOT film does not change the electrode processes at low potentials (i.e. the electrocatalyst is still blocked by CO_{ads}). At potentials above *ca*. 0.4 V (the potential at which CO_{ads} oxidation occurs), an enhancement in the electrocatalytic activity due to PEDOT can be seen in the large increase in MeOH oxidation peak currents (Fig. 5c) and the emergence of a second oxidation feature in HCOOH oxidation (Fig. 7c). This effect can be readily explained by an increased CO oxidation rate (Fig. 1, reaction 2) in the presence of PEDOT, reactivating previously blocked sites on the platinum surface at which MeOH or HCOOH can be turned over, and keeping these sites free by immediately oxidising any CO_{ads} formed through reactions 1 and 6.

There are multiple mechanisms through which PEDOT might enhance CO oxidation. One possibility is that PEDOT directly weakens the Pt–CO bond, either through modifying the electronic structure of the Pt NPs or by acting as a sink for CO, due to its lipophilicity. Alternatively, PEDOT might assist in activating water needed to oxidise CO. Finally, PEDOT may play a role in the NP deposition progress, steering it towards the formation of Pt NPs with different structural character which promotes CO oxidation. Unfortunately, it is not possible to distinguish between these mechanisms in the current study, but these would be worthwhile avenues to explore in the future in the view of the evident significant impact of PEDOT on the activity of Pt NPs. Furthermore, the role of PEDOT on the intermediates formed and product distribution also remains to be evaluated through further studies. This would be very challenging at the level of a small surface coverage of well-defined Pt NPs, but would be highly beneficial in terms of understanding and optimising this electrocatalytic system.

Conclusions

We have demonstrated that high densities of small isolated Pt NPs can be readily formed by electrodeposition at PEDOT-coated HOPG as a support. Thus, PEDOT acts not only as a conducting medium but also as a NP stabiliser preventing agglomeration in a similar way to other polymers such as block copolymers [53]. In contrast, the formation of discrete NPs on native HOPG is much more difficult to achieve: aggregates of NPs are formed typically, with a preference for NP formation at characteristic sites, such as step edges.

A significant finding in this work is that PEDOT has a large effect on the electrocatalytic activity of the NP: the electrocatalytic oxidation of MeOH is an order of magnitude faster when PEDOT is employed as a support for Pt NPs, compared with similarly prepared Pt NPs on native HOPG (based on the peak current density response). Similarly, HCOOH oxidation is enhanced at high potentials. We have attributed these findings to an enhanced oxidation rate of adsorbed CO in the presence of PEDOT. Thus, CPs show great promise as support materials for enhancing specific electrocatalytic reactions.

Although we have demonstrated enhanced electrocatalytic activity of Pt-PEDOT arrays, further work is needed to fully elucidate the mechanisms operating, including which intermediates are formed.

Finally, we point out that AFM image analysis has been proven as a valuable for determining the morphology, size and surface coverage of NPs, yielding results commensurate with voltammetric analysis of surface area. This was of particular importance in the present study, which often involved a low surface coverage of small NPs where more widely known techniques (charge from either the Pt oxide stripping peak or H_{ads}) sometimes proved difficult to implement.

Acknowledgements We are grateful to the following for support of this work: (1) equipment from Birmingham Science City (West Midlands centre for Advanced Materials, co-supported by the European Regional Development Fund; Hydrogen Energy Project); (2) COST D36; (3) the National Physical Laboratory (NPL) and EPSRC for support for HVP; (4) the EPSRC for support of SCSL, PRU and JVM (EP/H0239091); (5) Ministerio de Ciencia c Innovación (CTO2010-17127) and Junta de Castilla y León (GR-71, BU006A09); (6) the Academy of Finland (VR).

References

1. Chan K-Y, Ding J, Ren J, Cheng S, Tsang KY (2004) J Mater Chem 14:505–516
2. Steele BCH, Heinzel A (2001) Nature 414:345–352
3. Daniel M-C, Astruc D (2003) Chem Rev 104:293–346
4. Shan J, Tenhu H (2007) Chem Commun 44:4580–4598
5. Mayrhofer KJJ, Blizanac BB, Arenz M, Stamenkovic VR, Ross PN, Markovic NM (2005) J Phys Chem B 109:14433–14440

6. Scheijen FJE, Beltramo GL, Hoeppener S, Housmans THM, Koper MTM (2008) J Solid State Electrochem 12:483–495
7. Sánchez-Sánchez CM, Solla-Gullón J, Vidal-Iglesias FJ, Aldaz A, Montiel V, Herrero E (2010) J Am Chem Soc 132:5622–5624
8. Burda C, Chen X, Narayanan R, El-Sayed MA (2005) Chem Rev 105:1025–1102
9. Litster S, McLean G (2004) J Power Sources 130:61–76
10. Rao V, Simonov PA, Savinova ER, Plaksin GV, Cherepanova SV, Kryukova GN, Stimming U (2005) J Power Sources 145:178–187
11. Zhao Y, Yang X, Tian J, Wang F, Zhan L (2010) J Power Sources 195:4634–4640
12. Antolini E, Gonzalez ER (2009) Applied Catalysis A: General 365:1–19
13. Kulesza PJ, Chojak M, Karnicka K, Miecznikowski K, Palys B, Lewera A, Wieckowski A (2004) Chem Mater 16:4128–4134
14. Bensebaa F, Farah AA, Wang D, Bock C, Du X, Kung J, Le Page Y (2005) J Phys Chem B 109:15339–15344
15. Salavagione HJ, Sanchís C, Morallón E (2007) J Phys Chem C 111:12454–12460
16. Choi YS, Joo SH, Lee S-A, You DJ, Kim H, Pak C, Chang H, Seung D (2006) Macromolecules 39:3275–3282
17. Selvaraj V, Alagar M (2007) Electrochem Commun 9:1145–1153
18. O'Mullane AP, Dale SE, Macpherson JV, Unwin PR (2004) Chem Commun 14:1606–1607
19. O'Mullane AP, Dale SE, Day TM, Wilson NR, Macpherson JV, Unwin PR (2006) J Solid State Electrochem 10:792–807
20. Rice C, Ha S, Masel RI, Waszczuk P, Wieckowski A, Barnard T (2002) J Power Sources 111:83–89
21. Wang H, Löffler T, Baltruschat H (2001) J Appl Electrochem 31:759–765
22. Wang H, Wingender C, Baltruschat H, Lopez M, Reetz MT (2001) J Electroanal Chem 509:163–169
23. Léger JM (2001) J Appl Electrochem 31:767–771
24. Lebedeva NP, Koper MTM, Feliu JM, van Santen RA (2002) J Phys Chem B 106:12938–12947
25. Lai SCS, Lebedeva NP, Housmans THM, Koper MTM (2007) Top Catal 46:320–333
26. Markovic NM, Ross PN (2002) Surf Sci Rep 45:117–229
27. Capon A, Parsons R (1973) J Electroanal Chem 45:205–231
28. Capon A, Parsons R (1973) J Electroanal Chem 44:239–254
29. Wieckowski A, Sobkowski J (1975) J Electroanal Chem 63:365–377
30. Zhou W, Du Y, Zhang H, Xu J, Yang P (2010) Electrochim Acta 55:2911–2917
31. Patra S, Munichandraiah N (2008) Langmuir 25:1732–1738
32. Kuo C-W, Huang L-M, Wen T-C, Gopalan A (2006) J Power Sources 160:65–72
33. Vercelli B, Zotti G, Berlin A (2009) J Phys Chem C 113:3525–3529
34. Pandey RK, Lakshminarayanan V (2010) J Phys Chem C 114:8507–8514
35. Penner RM (2002) J Phys Chem B 106:3339–3353
36. Li Q, Brown MA, Hemminger JC, Penner RM (2006) Chem Mater 18:3432–3441
37. Bayati M, Abad JM, Nichols RJ, Schiffrin DJ (2010) J Phys Chem C 114:18439–18448
38. Lu G, Zangari G (2006) Electrochim Acta 51:2531–2538
39. Brülle T, Stimming U (2009) J Electroanal Chem 636:10–17
40. Ventosa E, Palacios JL, Unwin PR (2008) Electrochem Commun 10:1752–1755
41. Day TM, Unwin PR, Macpherson JV (2006) Nano Lett 7:51–57
42. Boxley CJ, White HS, Lister TE, Pinhero PJ (2002) J Phys Chem B 107:451–458
43. Walter EC, Zach MP, Favier F, Murray BJ, Inazu K, Hemminger JC, Penner RM (2003) ChemPhysChem 4:131–138
44. Li F, Ciani I, Bertoncello P, Unwin PR, Zhao J, Bradbury CR, Fermin DJ (2008) J Phys Chem C 112:9686–9694
45. Trasatti S, Petrii OA (1992) J Electroanal Chem 327:353–376
46. Doña Rodríguez JM, Herrera Melián JA, Pérez Peña J (2000) J Chem Educ 77:1195–1197
47. Cherstiouk OV, Simonov PA, Savinova ER (2003) Electrochim Acta 48:3851–3860
48. RodrIguez-Nieto FJ, Morante-Catacora TY, Cabrera CR (2004) J Electroanal Chem 571:15–26
49. Bayati M, Abad JM, Bridges CA, Rosseinsky MJ, Schiffrin DJ (2008) J Electroanal Chem 623:19–28
50. Bergamaski K, Pinheiro ALN, Teixeira-Neto E, Nart FC (2006) J Phys Chem B 110:19271–19279
51. Frelink T, Visscher W, van Veen JAR (1995) J Electroanal Chem 382:65–72
52. Chang SC, Leung LWH, Weaver MJ (1990) J Phys Chem 94:6013–6021
53. Kumar S, Zou S (2008) Langmuir 25:574–581